Aerospace Science and Technology 115 (2021) 106788

Contents lists available at ScienceDirect

Aerospace Science and Technology

www.elsevier.com/locate/aescte

Reduction of surface friction drag in scramjet engine by boundary layer combustion

Rui Xue [a,b,c,*], Xing Zheng [a], Lianjie Yue [b], Qian Zhang [a], Xin He [a], Jing Yang [a,c], Chao Weng [c,d], Zhihao Li [e]

[a] State Key Laboratory for Strength and Vibration of Mechanical Structures, Shaanxi Engineering Laboratory for Vibration Control of Aerospace Structures, School of Aerospace, Xi'an Jiaotong University, 710049 Xi'an, People's Republic of China
[b] State Key Laboratory of High Temperature Gas Dynamics, Institute of Mechanics, Chinese Academy of Sciences, 100190 Beijing, People's Republic of China
[c] The YuelaiYH Company, 550000 Guiyang, People's Republic of China
[d] Tongji University, 200092 Shanghai, People's Republic of China
[e] Xi'an Modern Control Technology Research Institute, 710065 Xi'an, People's Republic of China

ARTICLE INFO

Article history:
Received 15 September 2020
Received in revised form 20 February 2021
Accepted 26 April 2021
Available online 7 May 2021
Communicated by Cheng Wang

Keywords:
Boundary layer combustion
Skin-friction reduction
Supersonic combustion
Scramjet engine

ABSTRACT

This study investigates the effects of boundary layer combustion on skin friction reduction in a model scramjet combustor. The 4-equation RANS model (Transition SST model) is employed as the turbulence model and one experimental case which involves supersonic turbulent boundary layer combustion is used for validating the numerical simulation method. Then a wall jet device which can be used to inject hydrogen into boundary layer is designed and added to the lower wall of the combustor in the model scramjet engine. The numerical results showed that the optimal ratio between the primary fuel, producing thrust, and the wall jet fuel, used for drag reduction, for getting the largest skin-friction drag reduction when installing the wall jet device in the combustor, is 3:1. The study of modifying the location of the wall jet device showed that setting the wall jet position too close to the upstream or downstream could not get the maximum overall drag reduction. The installation position in the flow path depends on the coupling of primary fuel and wall jet fuel combustion. In practical scramjet design, the distribution ratio of primary to wall jet fuel and the location of wall jet device should be weighed to improve skin-friction reduction efficiency and overall engine performance.

1. Introduction

Scramjet engines have been considered to be one of the most appropriate propulsion systems for hypersonic air-breathing vehicles [1–4]. Though much advancement has been made in the development of the scramjet engine science and technology, realizing its practical engineering application is still a formidable task for several reasons. One of the reasons is the stringent frictional losses it confronts during hypersonic speeds. The experimental study carried out by Goyne et al. [5] concluded that skin-friction drag is the main degrader of scramjet combustor efficiency as skin friction drag becomes a significant proportion of overall vehicle drag at high Mach numbers. Among numerous skin-friction reduction techniques [6–12], boundary layer combustion proves to be an efficient way to reduce the skin-friction in turbulent flows. Stalker [13] established an analytical theory that could predict skin friction coefficient and heat flux factor based on Van Driest [14] compressible turbulent boundary layer model. It was found that the skin-friction drag reduction with mixing and combustion of the hydrogen was three times that in the case of mixing alone. Barth et al. [15] extended this model to make it be used for the analysis of other hydrocarbon fuels. Combustion characteristics in a supersonic combustor with hydrogen injection were investigated both experimentally and numerically by Song et al. [16,17]. Rowan et al. [18] carried out experimental study on skin-friction reduction of film-cooling by using porthole and slot injectors respectively. They found that at low equivalence ratios, the maximum skin-friction reduction was obtained by using porthole injector. Increasing the equivalence ratio could slightly increase the level of skin-friction reduction with slot injector. In order to verify the wall drag reduction performance by boundary layer combustion under different flight speeds, Suraweera et al. [19] conducted further experimental research on the base of Goyne's [5] investigation. Their results showed that through employing boundary-layer combus-

* Corresponding author at: State Key Laboratory for Strength and Vibration of Mechanical Structures, Shaanxi Engineering Laboratory for Vibration Control of Aerospace Structures, School of Aerospace, Xi'an Jiaotong University, 710049 Xi'an, People's Republic of China.
E-mail address: ruixue87@126.com (R. Xue).

https://doi.org/10.1016/j.ast.2021.106788
1270-9638/

tion, reductions for skin friction could be achieved at different flight Mach numbers. Compared with the level measured without hydrogen injection, the maximum reduction in skin friction coefficient could reach as high as 70% and 60% for high and low total enthalpy inflows respectively. Clark et al. [20] conducted a boundary layer combustion study with different type of fuel over a heated flat plate and the simulation results showed that hydrogen can achieve more effective skin friction reduction than JP-10. Volchkov et al. [21] carried out some experimental studies on the combustion characteristics of fuel injection in the laminar boundary layer. However, whether their conclusion could be extended into the scramjet engine in which the high-speed, strong turbulence of the boundary layer exists needs further studies to confirm. Recently, a numerical study conducted by Zhang et al. [22] showed that large skin-friction reduction could be obtained by boundary layer combustion, and further reduction could be achieved with adverse pressure gradient. Xue et al. [7,23] have carried out systematic numerical simulation and found that the skin friction could be reduced to 50% through boundary layer combustion while the pure-mixing case can only bring about 10% drag reduction. In the study of different factors on boundary layer combustion, it can be concluded that when shock waves interacted with the flame in boundary layer, in addition to reflection, they could also refract, which will cause the change of both skin friction and heat transfer on the wall as well.

In addition, some preliminary studies on the drag reduction characteristics of boundary layer combustion in scramjet environment have also been carried out. Trenker et al. [24] investigated the benefits of injecting fuel into the boundary layer in a simplified scramjet model, the effects of different locations for injection as well as the amount of fuel injected were explored. It was found that more H_2 must be injected and burned in the thicker boundary layer to achieve a given percentage reduction in viscous drag than for the thinner boundary layer. Rowan and Paull [25] investigated the effects of different locations and directions for boundary layer fuel injection in a scramjet combustor, and the results indicated that both strategies were equal in terms of heat release through combustion. In 2012, Kirchhartz et al. [26] conducted wind-tunnel experimental studies on the characteristics of drag reduction by boundary layer combustion under different leading edge configurations and pressure gradient conditions using a practical scramjet combustor. They found that at low-enthalpy flow, the combustion chamber friction resistance can be reduced up to 77% with employing blunt front edge configuration. Recently, Chan et al. [27] studied the applicability of the boundary combustion drag reduction technique in a scaling model scramjet engine. The effectiveness of skin friction reduction by boundary layer combustion under the airflow disturbance at the combustor entrance induced by the upstream inlet flow [28] or eddy generator [29] was validated by free-jet experiments. Their experimental data proved that the drag reduction effectiveness of the boundary layer combustion is nearly not influenced by the incoming flow conditions, and the total drag reduction level could reach as high as 61% in the combustion chamber. Wang et al. [30] analyzed the skin-friction in a rocket-based combined-cycle engine operating from Mach 1.5 to 6.0 by numerical simulations for whole engine flow path. Their results showed that the method of hydrogen combustion in boundary layer has achieved 57.7% skin-friction reduction effect.

It can be seen that the excellent features of boundary layer combustion for skin-friction reduction in supersonic flows have already been verified in previous studies. However, these studies are mostly conducted by using ideal models like the simple plate model, while the researches carried out in real scramjet combustor configurations and operation conditions are quite few. Furthermore, there are few studies on the coupling physical and chemical processes of boundary layer combustion to reduce surface friction in scramjet combustor. Therefore, in the present study, the impact of boundary layer combustion on skin friction reduction in actual scramjet environment will be carried out. Firstly, the physical model and simulation methodology is discussed in Section 2. Then in Section 3, the key factors like the inflow conditions and fuel injection for boundary layer combustion are conducted. Three different distribution ratios of the primary fuel that is used to produce thrust to the wall jet fuel that is used for skin friction reduction such as 2:1, 3:1 and 4:1 are chosen to investigate the interaction of the main-flow combustion and the boundary layer combustion. Other factors like the installation position of the wall jet device in the flow path on the wall drag reduction and engine performance are studied. Thus, by introducing boundary layer drag reduction technology into scramjet and the investigation on the influence of key factors on boundary layer combustion in real scramjet environment, the mechanism and the characteristics of boundary layer combustion for skin friction reduction can be obtained, which lays the foundation for further research on the application of the drag reduction technology in scramjet engines.

2. Numerical simulation methods and validation

2.1. Models and numerical schemes

The conservation form of the Reynolds-averaged Navier-Stokes equations with chemical reactions is given as follows:

$$\frac{\partial}{\partial t}\int_{\Omega}\vec{W}d\Omega+\oint_{\partial\Omega}(\vec{F}-\vec{G})\cdot d\vec{S}=\int_{\Omega}\vec{H}d\Omega \tag{1}$$

where the conservative variable vector is defined as

$$\vec{W}=(\rho,\rho u,\rho v,\rho w,\rho e,\rho Y_i) \tag{2}$$

$\vec{F}$ is inviscid vector fluxes, and $\vec{G}$ represents the item caused by the effects of viscosity, heat transport and component diffusion. $\vec{H}$ represents the chemical reaction source item. In Eq. (2), ρ is the density, u, v and w are the velocity components in the x, y and z directions, respectively. e is the total energy, and Y_i is the mass fraction of species i.

Transition SST model is a four-equation eddy-viscosity type, which is based on the coupling of the SST k–ω transport equations with two other transport equations, one for the intermittency and one for the transition onset criteria, in terms of momentum-thickness Reynolds number. An empirical correlation (Langtry and Menter) has been developed to cover standard bypass transition as well as flows in low freestream turbulence environments. It describes the transition process using the intermittency parameter γ. This parameter gives information about the fraction of time when the flow becomes turbulent.

The transport equation for the intermittency γ is defined as:

$$\frac{\partial(\rho\gamma)}{\partial t}+\frac{\partial(\rho U_j\gamma)}{\partial x_j}=P_{\gamma1}-E_{\gamma1}+P_{\gamma2}-E_{\gamma2}+\frac{\partial}{\partial x_j}\left[\left(\mu+\frac{\mu}{\sigma_r}\right)\frac{\partial\gamma}{\partial x_j}\right] \tag{3}$$

The transition sources are defined as follows:

$$P_{\gamma1}=C_{a1}F_{length}\rho S[\gamma F_{onset}]^{C_{\gamma3}} \tag{4}$$

$$E_{\gamma1}=C_{e1}P_{\gamma1}\gamma \tag{5}$$

where S is the strain rate magnitude, F_{length} is an empirical correlation that controls the length of the transition region, and C_{a1} and C_{e1} hold the values of 2 and 1, respectively.

In this paper, the laminar finite-rate model is used as the combustion model. For chemical kinetics, the 9-species, 27-reaction

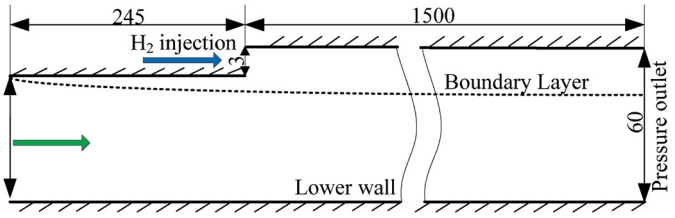

Fig. 1. Schematic of Suraweera et al.'s experiment [19].

Table 1
Inflow conditions for the airstream and injected fuel [19].

Parameter	Ma	T (K)	P (MPa)	Y_{O_2}	Y_{H_2}	Y_{N_2}
Airstream	4.42	1120	83	0.234	0	0.766
Hydrogen	1.93	170	49.5	0	1	0

model established by Marinov [31] is adopted as the hydrogen/air reaction mechanism. This chemical reaction mechanism has been proved appropriately for supersonic combustion flow simulation [32]. The reaction rate constant is approximated by the Arrhenius Equation:

$$k = AT^B \exp(-E/RT) \tag{6}$$

where A is the pre-exponential collision frequency factor, T represents the temperature and B means the temperature exponent. E is the activation energy, and R represents the gas constant.

Roe-FDS splits the fluxes in a manor that is consistent with their corresponding flux method eigenvalues. The Roe flux-difference splitting (Roe-FDS) was selected for the fluxes calculation. The Second Oder Upwind Scheme was used for spatial discretization of the scalars. Various key parameters were monitored to determine the convergence, namely: 1) The residual error should be 3 to 4 orders of magnitude smaller than the initial value. 2) The time history of mass flux of H_2O at the exit should nearly remain constant. 3) The relative mass flow rate error, $|\dot{m}_{out} - \dot{m}_{in}|/\dot{m}_{in}$, was on the order of $\times\ 10^{-7}$.

2.2. Validation of the numerical simulation method

In this study, an experimental case conducted by Suraweera et al. [19] in 2005 is selected to validate the adopted numerical methods, which includes the H_2 injection and combustion in supersonic turbulent boundary layer. Fig. 1 shows the configuration of the experimental case. The whole configuration is comprised by an entrance section and test section. The entrance section is 245 mm long with 57 mm height, and it is terminated by a 3 mm rearward facing step where hydrogen can be injected along the flow direction. Downstream the step, there is a 1500 mm long test section. Due to the symmetry in spanwise direction, the numerical simulation is conducted in two dimensions and the structural mesh is given in Fig. 2. Meshes in domains around the wall and near the mixing layer are refined. The inflow conditions extracted from [19] are listed in Table 1. In addition, the no-slip condition is used and the wall temperature is kept at $T_W = 300$ K for both the upper wall and lower wall. As for the outlet, all the physical variables are extrapolated from the internal cells.

The temperature and Mach number contours are given in Fig. 3, respectively. It can be seen that the fuel is spontaneously to be ignited in the boundary layer at some distance away the downstream of the step. Then the high-temperature boundary layer gradually thickens with the mixing between the core flows. It can be concluded from the Mach number distribution that within the high-temperature boundary layer at the downstream on the upper wall, the Mach number is above 1 in most part of this region, which means the combustion occurs in supersonic velocity in boundary layer.

The skin friction coefficient is presented in a proportional reduction form based on results from the no injection case. Equation (7) shows how the skin friction coefficient $C_{f,i}$ was calculated. All skin friction coefficients presented here are based on local freestream conditions.

$$C_{f,i} = \frac{2\tau_w}{\rho U^2} \tag{7}$$

where the shear stress τ_w was a local value obtained at point i along the test surface, the velocity U and density values ρ used in Equation (7) were freestream values.

Fig. 4 shows the skin friction coefficient in proportional form as calculated based on computational results, in comparison to the experimental results obtained from Suraweera et al. [17]. $C_{f,\text{mix}}$, $C_{f,\text{com}}$ and $C_{f,\text{no-injection}}$ represent the skin friction coefficient at the pure-mixing, combustion and no fuel injecting conditions, respectively. A value of 1 in the proportional reduction form corresponds to no change in the skin friction coefficient (equal to no-injection case) and a value of 0 corresponds to a 100% reduction in the skin friction coefficient. It can be seen that the numerical results both in the mixing and combustion cases are controlled within experimental error. It is obvious that the whole skin-friction variation process can be divided into two regions for both mixing only and combustion conditions. In Reg. 1 which is close to the injector, it is primarily in laminar flow as the injected fuel flow just starts to develop along the wall surface. So the film cooling plays a major role in this region and the relative skin-friction coefficient (to no-injection case) decreases along the wall. Near the end of Reg. 1 at about $x = 0.06$ m, the relative reduction of skin-friction coefficient can reach as high as 60% and 70% for mixing and combustion cases, respectively. After that, the boundary layer transition occurs and the skin-friction coefficient gradually increases. As the whole boundary layer turns to be turbulence flow, the skin-friction coefficient tends to be the constant value. The process of this skin-friction coefficient variation with the change of flow characteristics along the wall has been also mentioned in reference [7]. Therefore, from this variation process it can be concluded that because of the self-ignition delay of the injected fuel, the influence of boundary layer combustion is mainly in the downstream turbulence region. The addition of boundary layer combustion can make the skin-friction coefficient decrease larger than 50% while the mixing only case can bring little reduction for wall stress at the downstream.

Suraweera et al. also quantified changes in the Stanton number as a result of boundary layer combustion. They calculated the local Stanton number using the heat transfer measurements from thin-film gauges. The Stanton number is defined in Equation (8) [19].

$$c_h = \frac{\dot{q}}{\rho U(H_{aw} - H_w)} \tag{8}$$

where $\dot{q}$ is the measured heat flux, ρ is the freestream density, U is the freestream velocity, and H_{aw} and H_w are the adiabatic wall and wall enthalpies, respectively.

The effect of boundary layer combustion to the wall heat transfer is extracted and shown in Fig. 5. $C_{h,\text{com}}$, $C_{h,\text{mix}}$ and $C_{h,\text{no-injection}}$ are the Stanton numbers for combustion, pure-mixing and no-injection cases, respectively. The value of Stanton number distributions for the both combustion and mixing case are in good agreement with the experimental results, and most of them are controlled within the experimental error range. The experimental accuracy of heat transfer was estimated as $\pm 10\%$. The numerical simulations for the combustion case at this test condition overestimate the level of Stanton number in the downstream ($x > 1.0$

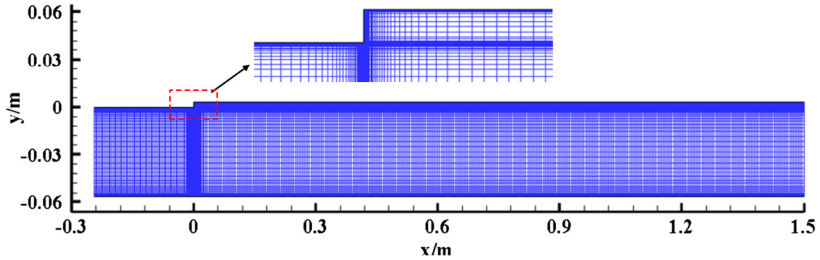

Fig. 2. The computational grids of the configuration.

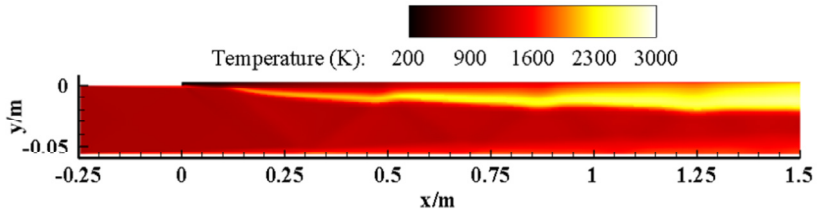

(a) Temperature

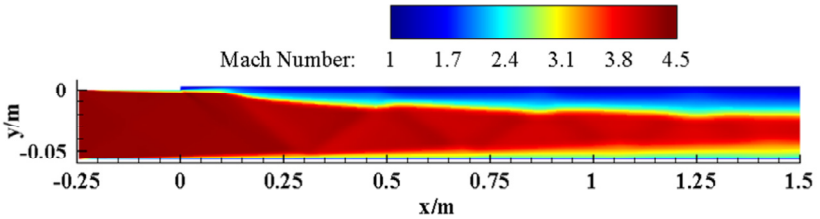

(b) Mach number

Fig. 3. Temperature (a) and Mach number (b) contour for Suraweera's experiment. (For interpretation of the colors in the figure(s), the reader is referred to the web version of this article.)

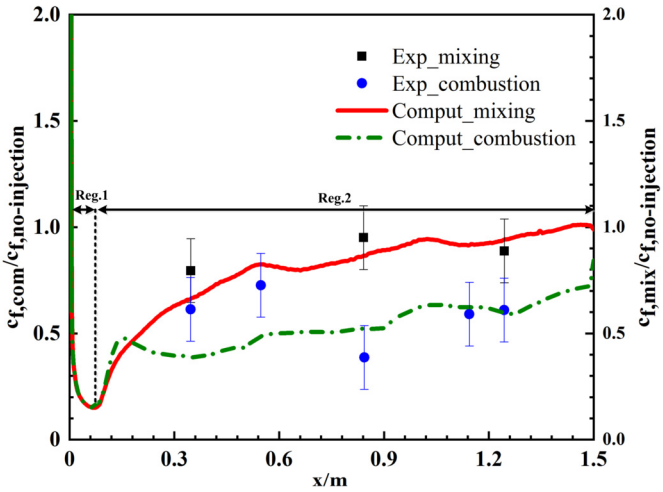

Fig. 4. Influences on C_f between pure-mixing and combustion cases.

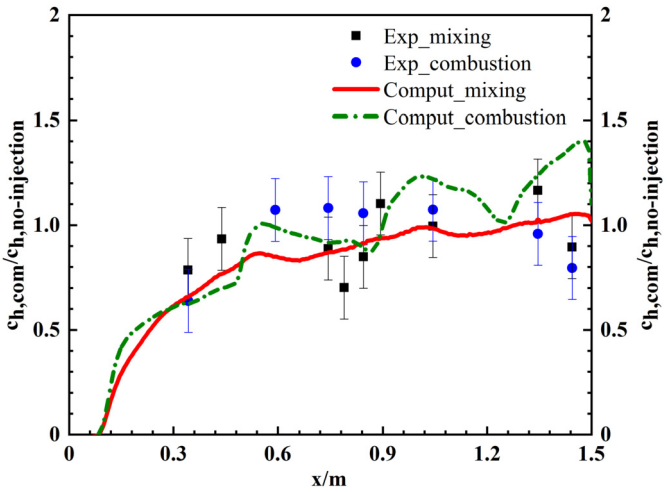

Fig. 5. Influences on C_h between pure-mixing and combustion cases.

m), which also could be an indication of the process of forming that water. Moreover, the possible reason for this deviation is that when combustion occurs in boundary layer, the measurement of heat transfer on the wall is quite difficult. So the accuracy of measurement cannot be guaranteed for the combustion case. The effects of elevated temperature from combustion were offset by the pronounced lowering of the near wall gradients.

The agreements on the distribution of both skin friction and heat transfer along the flow path prove that the numerical method employed in this paper can reproduce the flow field with supersonic mixing and combustion and accurately predict the skin friction and heat transfer with boundary layer combustion. The comparisons between the computational and experimental results in Fig. 5 illustrate that the RANS simulations well reproduce the influence tendencies on the skin friction and heat transfer by boundary-layer mixing and combustion revealed by the experimental data. Therefore, this numerical method will be used in the subsequent section to study application of boundary layer combustion for the reduction of skin friction in one scramjet combustor model.

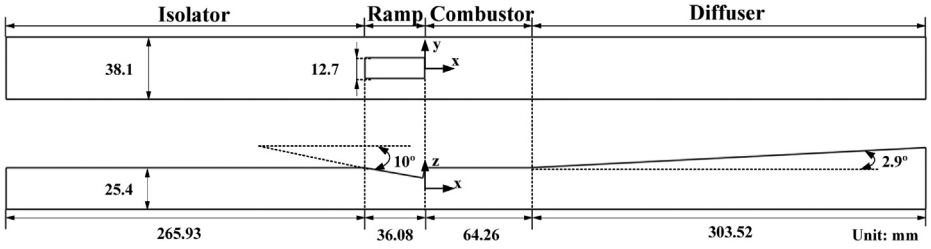

Fig. 6. Schematic of Virginia supersonic combustion facility.

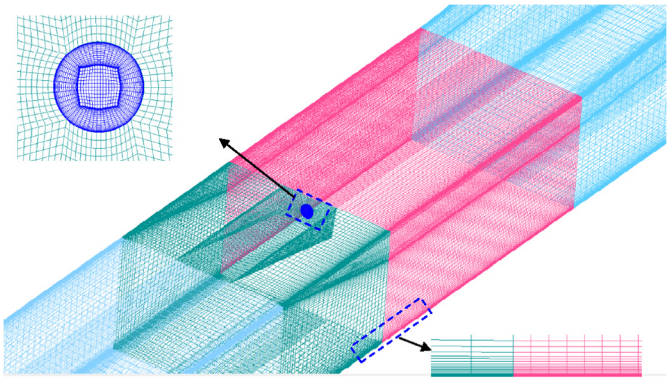

Fig. 7. Sample structured mesh with close views at encrypted area.

3. Analysis and discussion

A scramjet combustor model which is based on the experimental configuration of the University of Virginia's (UVA) Supersonic Combustion Facility is used for the study of boundary layer combustion in real scramjet engine [33]. Fig. 6 depicts the schematic diagram of this scramjet engine. The whole engine is in rectangular configuration. The cross section of the isolator is constant and its area is 38.1×25.4 mm^2. The fuel ramp with an angle of 10° into the airflow is used for fuel injection to burn and provide thrust. Its width is 12.7 mm and the normal height is 6.35 mm. At the exit of the combustor, the top wall diverges at a 2.9° angle to the diffuser exit. The width of the combustor model is constant and equal to 38.1 mm. A structured, three-dimensional, hexahedral grid consisting of ~1.6 million cells, divided among 31 zones was applied to the scramjet geometry using ICEM CFD. An overview of the structured grid is shown in Fig. 7.

The University of Virginia has carried out extensive experimental tests with this combustor model, which includes the data of Pitot pressure and stagnation temperature that are taken along the centerline of the top wall. It should be noted, from Fig. 6, that this domain covers only part of the entire UV "A" scramjet configuration, namely the isolator, combustor, and Diffuser, and excludes the upstream Mach 2 converging-diverging nozzle. Instead, as can be seen in Fig. 6, a uniform flow of air consisting of only streamwise velocity component of 1033 m/s (corresponding to a Mach 2 flow based on the mass flow rate $\dot{m} = 0.220$ kg/s and thermodynamic state of total pressure $p_0 = 327.72$ kPa) is imposed at the inflow plane. The fuel-injection is described by a mean uniform flow of pure hydrogen with both streamwise and wall-normal velocity components of 1770 m/s and −220 m/s, respectively, corresponding to a Mach 1.7 condition based on mass flow rate $\dot{m} = 0.00154$ kg/s and total temperature of 298 K, respectively. The global equivalence-ratio that corresponds to these inflow conditions is 0.260, indicating a fuel-lean combustion regime. All walls that envelope the computational domain are prescribed with a no-slip condition and have constant wall-temperature of $T = 600$ K in the non-reacting simulation. In the combusting case, the portion of the top wall and the ramp face have another isothermal condition of $T = 1000$ K. The inlet conditions for both the no injection and the combustion are defined in Table 2. Case 1_cold represents the no-injection case in which no fuel is injected into the airflow, while Case 2_combust_wo was run with fuel injection through the fuel ramp and combustion.

Three different grids are selected for grid independent verification. The grid information is shown in the Table 3. N and y_1 in the table represents the number of grid cells and the height of the first layer grid, respectively.

For Case 1_cold and Case 2_combust_wo conditions, three grids were respectively used to compare the pressure distribution at the downwall. And the comparison numerical results are shown in the Fig. 8. From the plot, the result of pressure at the downwall do not exhibit any major difference in Fig. 8(b), but the another result shows the consistency between medium and dense grid. And it is clear that the variation of grid scale has great influence on the region near the pressure fluctuation, so the verification of grid independence is very necessary for the study of skin-friction reduction in this paper. As such, the simulation is independent with the grid increasing when the number of grid reaches a moderate level. Hence, a medium grid is adopted in the subsequent numerical analysis.

Data of static pressure measured along the centerline of the top wall is shown in Fig. 8 for both no-injection and combustion cases. The x-axis is non-dimensioned by the normal height of fuel ramp region of engine, while the y-axis is normalized by the pressure value at the inlet of combustor. The simulation results agree with the experimental data for the Isolator and Combustor, discrepancies between the simulation result and the experimental data start to have greater variance in the diverging the nozzle under the two Cases. The section where the simulation results do not agree with experimental data is approximately at $x/H = 30$ through $x/H = 45$ for Case 1_cold. This is probably due to incorrect predication of the separated air flow on the top wall of the Diffuser. The discrepancy for Case 2_combust_wo occurs within the exit nozzle downstream of $x/H \approx 25$. The higher static pressures for the simulations in this region are likely due to the flow separation evident in Fig. 9 (Density Gradient contour). The reason for this numerically-induced phenomenon is still unclear and further investigation is necessary. It was hypothesized that it may be due to the outflow boundary condition treatment and the lack of conjugate heat transfer modeling at the wall boundaries.

As there is no combustion in case 1_cold, the fluctuations of pressure in the downstream of the isolator are significant which is induced by the shock wave reflection and the expansion waves produced by the protruding of fuel ramp into the main flow. This can also be illustrated in Fig. 9(a) for the Density Gradient contour, meanwhile, the X Velocity contour is also presented in Fig. 9(b).

Hydroxyl mass fraction contour with an isotherm at 1600 K in Fig. 10(a) show the general structure of the core flame. Moreover, one indication of possible mixing is turbulent kinetic energy (TKE). The Density Gradient contour in Fig. 10(b) shows the shock wave structure. Compared with Fig. 9(a), the shock wave forms a shock train between the shear layer and the lower wall of the main fuel and runs through the whole straight combustor. Meanwhile, be-

Table 2
Inflow conditions for the airstream and injected fuel.

Parameter	$\dot{m}$ (kg/s)	T_0 (K)	P_0 (kPa)	Y_{O_2}	Y_{H_2}	Y_{N_2}	φ
Case 1_cold							
Air	0.220	1033	327.72	0.232	0	0.768	0
Main fuel	0	0	0	0	0	0	
Case 2_combust_wo (without boundary layer combustion)							
Air	0.203	1203	326.97	0.232	0	0.768	0.260
Main fuel	0.00154	298.96	709.94	0	1	0	

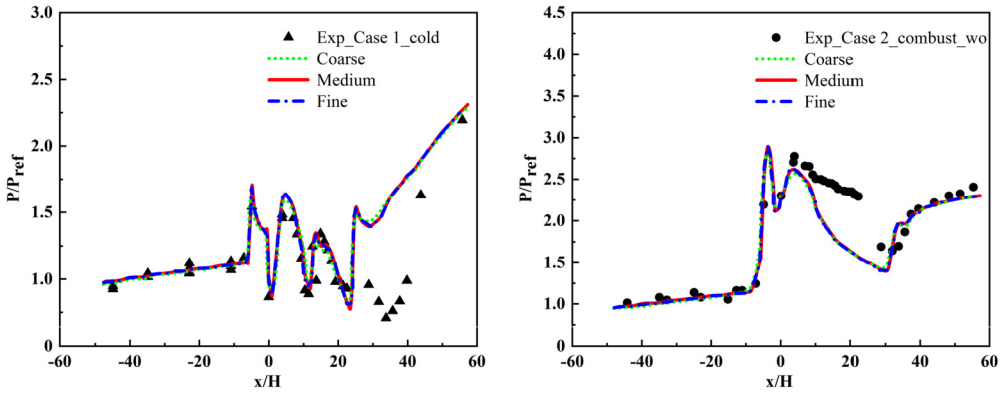

Fig. 8. Pressure distribution along axial centerline of top wall for Case 1_cold **(a)** and Case 2_combust_wo **(b)** of three grid solutions.

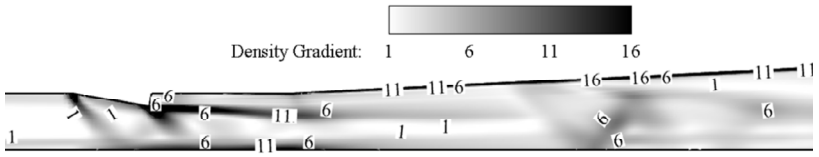

(a) Density Gradient

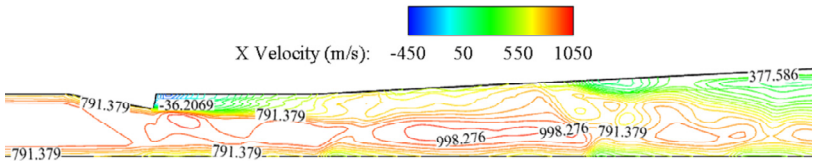

(b) X velocity

Fig. 9. Density Gradient (a) and X velocity (b) contour on the symmetry plane ($y = 0$) for Case 1_cold.

Table 3
Meshes used to verify the grid independence.

Name	Coarse	Medium	Fine
N	45023	306453	403123
y^+	3	1	1
y_1	10^{-5}	10^{-6}	10^{-6}

cause the higher back pressure at the exit propagates along the low velocity boundary layer on the upper wall and leads to the separation of the boundary layer at a certain position, the oblique shock wave produced by it interacts with the supersonic flow on the lower wall, resulting in a second shock train of low height and intensity in the expansion section. In fact, TKE is associated with eddies in turbulent flow that then promotes mixing. The red areas on the contour plots represent areas of TKE that equal to or greater than 40,000 J/kg. A high TKE in the flow is found in the Fig. 10(c), which is caused by the counter-rotating vortices generated by the ramped injector rapidly mix fuel and air.

3.1. The addition of boundary layer combustion in scramjet combustor

As shown in Fig. 11, in order to investigate the effect of boundary layer combustion in real scramjet combustor, the above UVa combustor model is modified in which a wall jet device is designed and installed at the lower wall. Thus, the fuel that is used for boundary layer combustion can be tangentially injected into the boundary layer along the lower wall through a row of 5 holes at the base of the wall jet device. The height of wall jet device is 1.5 mm, the diameter of the holes was 0.5 mm and the distance between adjacent holes was 8 mm. Meanwhile, in order to distinguish the ramp injector on the upper wall which is used to produce thrust in the original combustor, in this new combustor model, the ramp fuel injector is indicated as Injector_1 and the added wall jet device on the lower wall which is used for boundary layer combustion is named as Injector_2. For the boundary conditions of Injector_2, the velocity of the injected fuel is kept Ma 1 for all holes and the total temperature is set as 298 K.

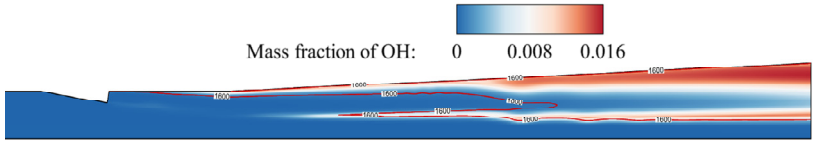

(a) Static pressure

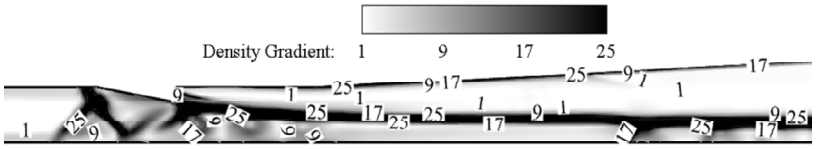

(b) Density Gradient

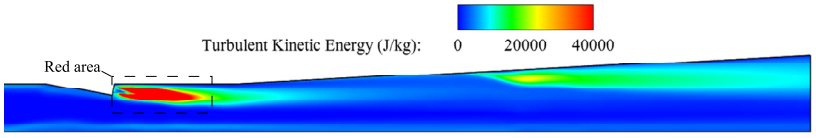

(c) Turbulent kinetic energy

Fig. 10. Static pressure (a), Density Gradient (b), and Turbulent kinetic energy (c) contour on the symmetry plane ($y = 0$) for Case 2_combust_wo.

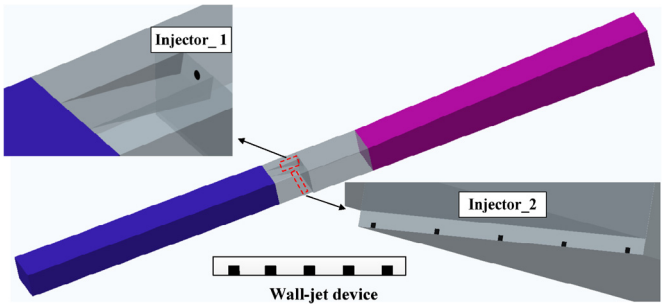

Fig. 11. Configuration of add the wall jet device.

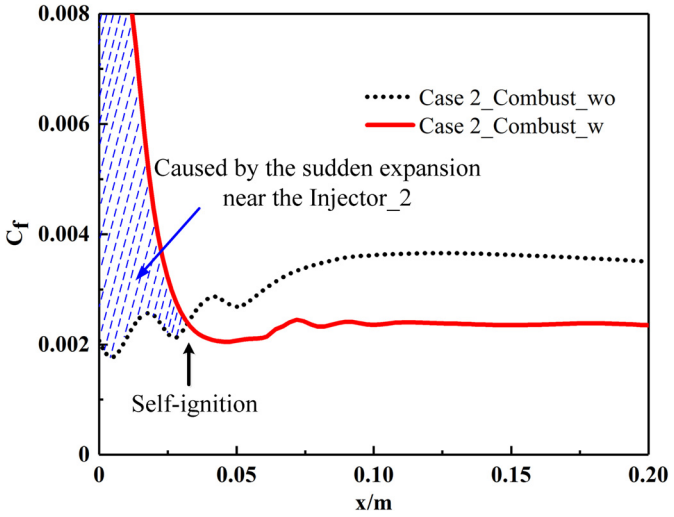

Fig. 12. Influences on C_f at midline on lower wall by boundary layer combustion.

Hydrogen is also used as the wall jet fuel and its injection equivalent ratio is set as 0.260. This case is also defined as BSL later (Baseline Case). Fig. 12 shows the distributions of skin-friction coefficient along the centerline of the lower wall with (Case 2_combust_w) and without boundary layer combustion (Case 2_combust_wo) respectively and in these two cases the total equivalent ratios of hydrogen is kept the same as 0.260. It can be seen that from $x = 0$ to $x = 0.03$ m, the skin-friction coefficient of Case 2_combust_w is larger than that of Case 2_combust_wo. The reason for this is that the addition of Injector_2 makes a sudden expansion of the flow path near the lower wall, which destroys the boundary layer flow structure developed from the upstream. Then near $x = 0.03$ m, the fuel is spontaneously ignited. The combustion of wall jet fuel made the skin friction rapidly reduce. As illustrated in reference [4] and [29], the primary reason for skin-friction decrease is that the density gradient can be significantly reduced as the addition of heat release with boundary layer combustion. The near wall velocity gradient and hence skin friction was observed to decrease markedly from cases where there was no combustion. These changes were largely attributed to alterations to the local mean density and viscosity.

For Case 2_combust_wo, as illustrated in Fig. 13(a), a quasi-normal shock wave is generated at the leading edge the fuel ramp and a shock train is then formed at downstream and extended to the outlet of the combustor. After that, due to the expansion of upper wall of the nozzle, the flow is accelerated. Meanwhile, as the ambient pressure at the exit is relatively high, it propagates forward through the low-velocity boundary layer on the upper wall. So near the middle of the nozzle section, the boundary layer is separated and a shock wave is produced. As the shock wave contacts and interacts with the high velocity flow near the lower wall, another shock wave is generated, which makes the pressure on the lower wall gradually increase to match the ambient pressure at the outlet of the flow channel.

Fig. 13(b) is the Mach number distribution for Case 2_combust_w of the center plane. Compared with Case 2_combust_wo, though the total equivalence ratio is the same, the leading edge of the shock train moves upstream to the isolator section when boundary layer combustion is added. One of the interesting characteristics of this scramjet model is the presence of a shock train that is produced by combustion and travels upstream into the isolator in Case 2_combust_w. The isolator then has to be long enough to prevent the shock train from traveling upstream to the inlet and

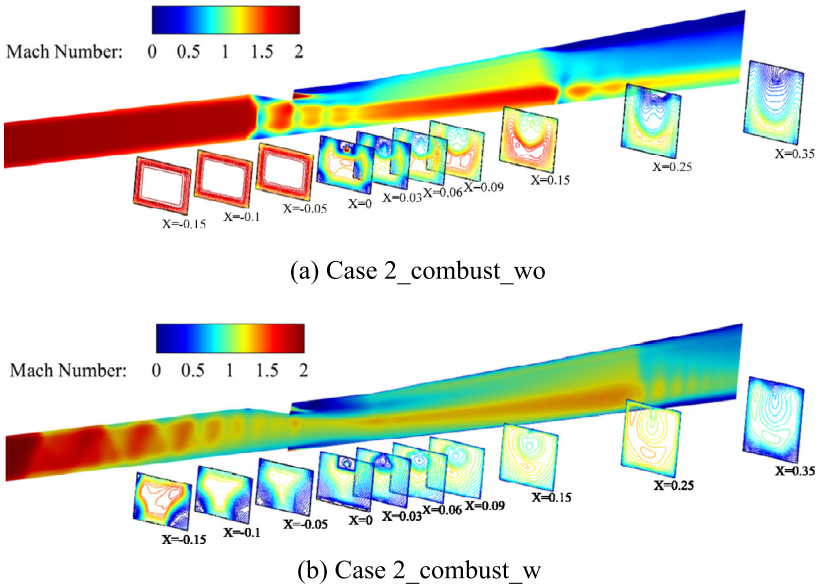

Fig. 13. Mach number contours for Case 2 with (a) and without (b) boundary layer combustion.

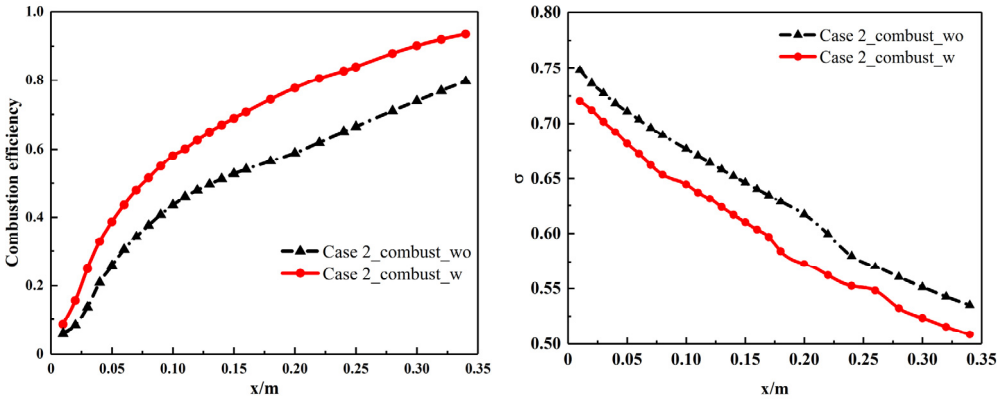

(a) Combustion efficiency (b) Total pressure recovery coefficient

Fig. 14. Combustion efficiency (a) and total pressure recovery coefficient (b) along the flow path for Case 2.

causing the engine to unstart. Moreover, in order to further analyze whether the addition of boundary layer combustion can bring great impact on the overall performance of the scramjet engine, the total pressure recovery coefficient σ and combustion efficiency are provided in next analysis.

The combustion efficiency, which is one of the key performances for scramjet evaluation is used. It is defined as the ratio of hydrogen fuel consumption rate to the hydrogen fuel supply rate and it is expressed as the following:

$$\eta_{\text{comb}}(x) = 1 - \frac{\int (A(x)) u \rho Y_{H_2} dA}{\dot{m}_{H_{2,inj}}} = 1 - \frac{\dot{m}_{H_{2,x}}}{\dot{m}_{H_{2,inj}}}$$

where, $\dot{m}_{H_{2,inj}}$ and $\dot{m}_{H_{2,x}}$ denote the mass flow rate of H_2 at the combustor inlet and at a streamwise station x.

In addition, the total pressure recovery coefficient σ is used to evaluate the total pressure loss during the combustion process, which is defined as

$$\sigma = \frac{\int P_{0,x} \rho u dA}{\int P_{0,inlet} \rho u dA}$$

where, $P_{0,inlet}$ is the inlet total pressure, $P_{0,x}$ is the local total pressure at a given section x.

From the Fig. 14, the combustion efficiency was enhanced with the boundary layer combustion, but the total pressure recovery factor was reduced. From the Fig. 14(a), it is observed that the overall combustion efficiency rise in the scramjet engine due to wall jet combustion is approximately 1.1–1.5 times that of observed when only the primary fuel is injected. This is mainly due to the fact that the fuel cannot be fully burned with the mainstream through the injection on the ramp, and the addition of boundary layer combustion makes the overall combustion more uniform, which can be shown in the apparent heat release rate (AHHR) distribution in Fig. 15. Moreover, at the outlet, the total pressure recovery coefficient decreased by 2% from 0.53 to 0.51. In combination with the Mach number contour shown in Fig. 13, it should be noted that the closer the shock wave is to the inlet of the flow passage, the greater the energy loss. In severe cases, the engine may not even start properly. On the whole, combustion efficiency or total pressure recovery coefficient cannot be used alone to optimize the design target of the combustor. Thus, when boundary layer combustion device for skin-friction reduction is introduced into the scramjet combustor, more consideration should be taken into account on the close interaction between isolator and combustor to achieve the overall optimal performance for the flow path.

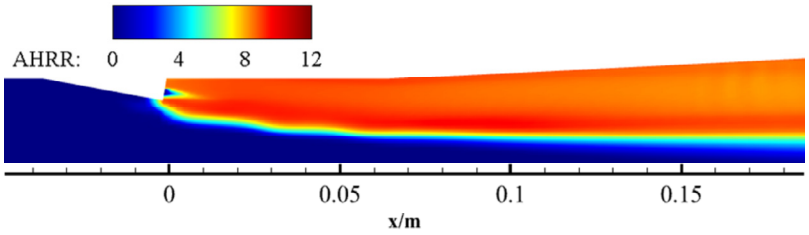

(a) Case 2_combust_wo

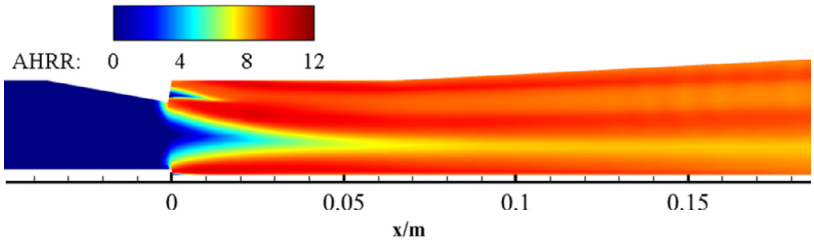

(b) Case 2_combust_w

Fig. 15. AHRR on the symmetry plane ($z = 0$) along the flow path for Case 2.

Fig. 16 shows the temperature contours on different cross sections along the flow path for Case 2. It can be seen that a large annular high-temperature reaction mixing layer is formed near the primary fuel injector at $x = 0.05$ m. Then with entrainment of the airflow into the mixing layer and mixes with the primary fuel, this annular mixing layer gradually expands inside and outside. Finally, a circular high-temperature region is formed at the downstream of the flow path close to the expansion wall. For boundary layer combustion, upstream of $x = 0.05$ m, edges of each reaction mixing layer generated by wall jets begin to merge as the distance between the wall jet fuel injection holes are not too far. The intermediate three annular flames within the boundary gradually disappear due to the entrainment and combustion with the air outside the boundary layer. Meanwhile, as the recirculation regions are formed near the corner area of sidewalls, the high-temperature regions induced by the wall jets near the side wall are gradually concentrated, which makes the side walls be subjected to severe thermal protection requirements. Therefore, in the following study of applying boundary layer combustion to the wall friction reduction of scramjet combustor, the relative position of main fuel and boundary layer fuel, the position between wall jet and the side wall needs to be carefully taken into account.

3.2. Influence of distribution ratio of primary to wall jet fuels

After verifying that the boundary layer combustion technique is applicable to scramjet for drag reduction, the influences of different factors such as the fuel distribution ratio (Cases 3 and 4) and injection location (Cases 5 and 6) are investigated. Table 4 describes the airstream and fuel injection conditions of different distribution ratio for primary to wall jet fuel.

Firstly, the effect of different distribution ratio ($\dot{m}_{\text{Injector\_2}}/\dot{m}_{\text{Injector\_1}}$) is investigated. In this study, the total amount of fuel injected into the scramjet combustor is kept constant. For the BSL case, the fuel injected into the boundary layer of the combustor is 25% of the total amount of fuel and the corresponding $\dot{m}_{\text{Injector\_2}}/\dot{m}_{\text{Injector\_1}}$ ratio is 1:3. Case 3 represents that the fuel injected into the boundary layer of the combustor is 20% of the total amount of fuel ($\dot{m}_{\text{Injector\_2}}/\dot{m}_{\text{Injector\_1}}$ ratio is 1:4) while Case 4 shows that the fuel injected by Injector_2 accounts 33.33% for of the total fuel ($\dot{m}_{\text{Injector\_2}}/\dot{m}_{\text{Injector\_1}}$ ratio is 1:2).

Fig. 17(a) shows the wall shear stress on the lower wall in the combustor for $\dot{m}_{\text{Injector\_2}}/\dot{m}_{\text{Injector\_1}}$ ratio from 1:4 to 1:2 respectively. With the increase of $\dot{m}_{\text{Injector\_2}}/\dot{m}_{\text{Injector\_1}}$ ratio, the wall shear stress is first decreases and then increases. The averaged value of the shear stress on the lower wall reaches its minimum when $\dot{m}_{\text{Injector\_2}}/\dot{m}_{\text{Injector\_1}}$ ratio is 1:3. As the value of shear stress on the lower wall is 293.97 Pa when hydrogen is not injected into boundary layer, adding boundary layer combustion can realize skin-friction reduction to as high as 29.34% when keeping the $\dot{m}_{\text{Injector\_2}}/\dot{m}_{\text{Injector\_1}}$ ratio to 1:3 while the other two cases can obtain 20.93% (Case 3) and 25.86% (Case 4) reduction respectively as shown in Fig. 17(b).

Fig. 18 represents the distributions of the skin-friction coefficient along the lower wall for different $\dot{m}_{\text{Injector\_2}}/\dot{m}_{\text{Injector\_1}}$ ratios. It could be noticed that the whole variation trends for all three cases are basically consistent and the changing process of skin friction coefficient along the flow path could be divided into three regions: in the first region (Reg. 1, $0 < x < 0.02$ m), as no combustion occurs (which can be seen from the temperature contour in Fig. 19(a)), the decrease of skin friction is mainly due to the fact that the Ma 1 injection of wall jet fuel can increase the flow velocity within the boundary layer which can effectively reduce the velocity gradient. Meanwhile, the density of hydrogen is lower than air, so two factors together make the wall shear stress reduce along the lower wall. As the ignition delay time for hydrogen is constant at the same environment and the wall jet injecting velocity is almost the same for these three cases, near $x = 0.02$ m, the fuel injected into boundary layer is auto-ignited for all these three cases. Then boundary layer combustion occurs and the skin frictional resistance of the lower wall gradually rises in the second region (Reg. 2, 0.02 m $< x <$ 0.17 m). The primary reason for the skin friction increase is that when boundary layer combustion just starts, the turbulent transport process between the core flow and boundary layer flow is sharply intensified which leads the shear stress on the wall be magnified. As the boundary layer flow moves downstream, due to the effect of boundary layer expansion induced by heat release from combustion, the added heat causing an expansion of the boundary layer and lowering of the wall shear

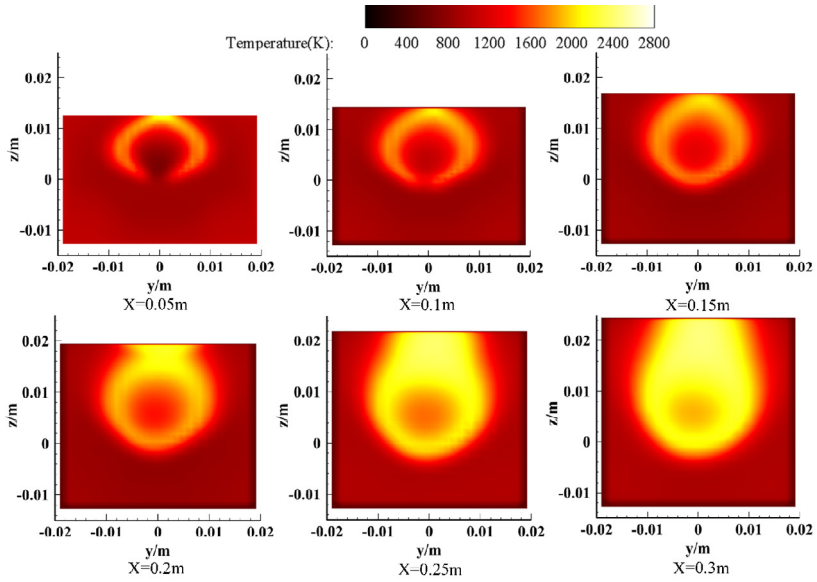

(a) Case 2_combust_wo

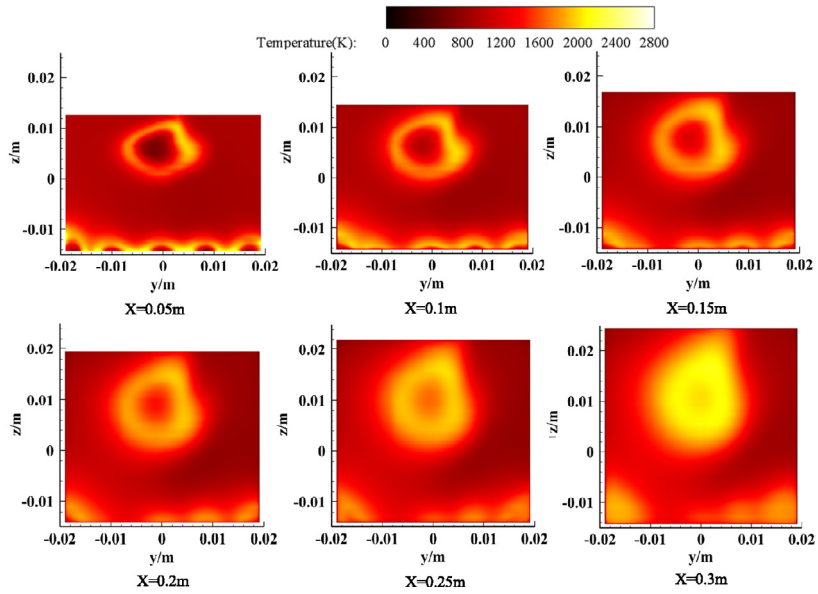

(b) Case 2_combust_w

Fig. 16. Temperature contours for Case 2 with (a) and without (b) boundary layer combustion.

Table 4
Inflow conditions of the airstream and injected fuel for BSL, Cases 3 and 4.

Parameter	$\dot{m}$ (kg/s)	T_0 (K)	P_0 (kPa)	Y_{O_2}	Y_{H_2}	Y_{N_2}	φ
BSL/Case 2_combust_w (with boundary layer combustion)							
Air	0.203	1203	327.72	0.232	0	0.768	
Injector_1	0.001155	297	709.94	0	1	0	0.260
Injector_2	0.000385	297	433.49	0	1	0	
Case 3							
Air	0.203	1203	326.97	0.232	0	0.768	
Injector_1	0.001232	298.96	709.94	0	1	0	0.260
Injector_2	0. 000308	298	301	0	1	0	
Case 4							
Air	0.203	1203	326.97	0.232	0	0.768	
Injector_1	0.001027	297	568.46	0	1	0	0.260
Injector_2	0. 000513	297	300	0	1	0	

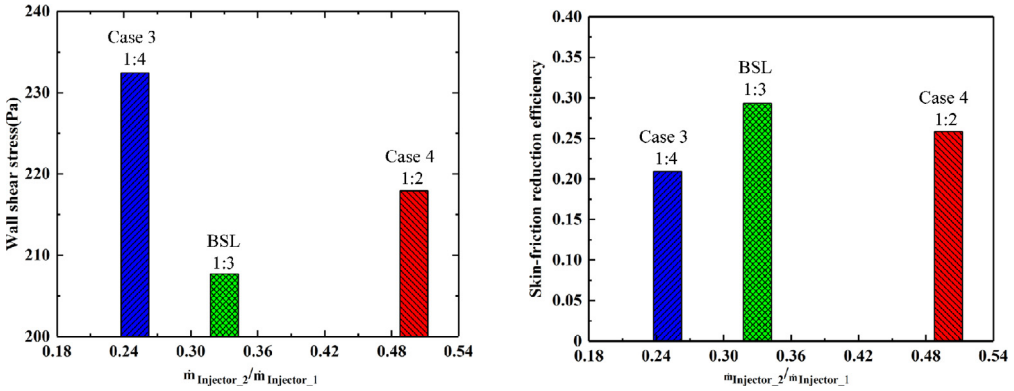

(a) Total wall shear stress (b) skin-friction reduction efficiency

Fig. 17. Comparison of Total wall shear stress (a) and skin-friction reduction efficiency (b) vs $\dot{m}_{Injector\_2}/\dot{m}_{Injector\_1}$.

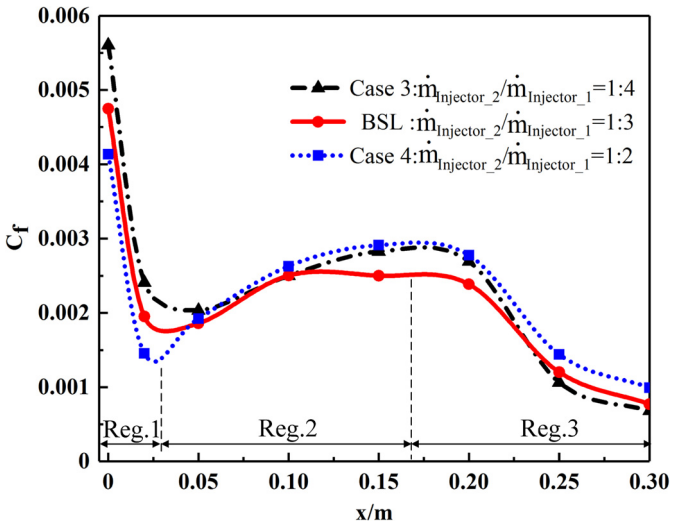

Fig. 18. Comparisons of C_f of lower wall for different $\dot{m}_{Injector\_2}/\dot{m}_{Injector\_1}$.

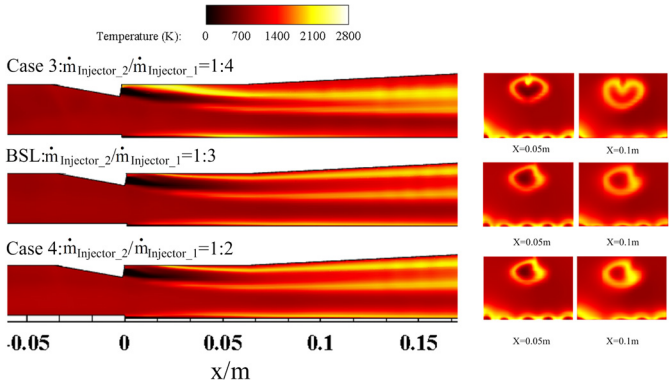

Fig. 19. Temperature contours of $y = 0$ for different distribution ratio.

stress, the velocity gradient within boundary layer and the corresponding frictional resistance coefficient is gradually decreased for the third region (Reg. 3, $x > 0.17$ m). It is this expansion that also results in lowering of the magnitude of the turbulent fluctuations and hence the vorticity of the flow.

So it could be concluded that in Reg. 1 where the film-cooling effect dominates, increasing the $\dot{m}_{Injector\_2}/\dot{m}_{Injector\_1}$ ratio is benefit for skin-friction reduction as more low-density, uniform velocity distribution fuel is injected into boundary layer. In the second and third regions, however, the drag reduction effect does not increase monotonically with the injection of the wall jet fuel due to the complicated interaction of turbulence and combustion. It can be seen that the best skin friction reduction could be achieved under the case of BSL ($\dot{m}_{Injector\_1}/\dot{m}_{Injector\_2}$ ratio $= 3$) while near the exit, Case 3 ($\dot{m}_{Injector\_1}/\dot{m}_{Injector\_2}$ ratio $= 4$) is approximate to achieve the optimal skin friction reduction.

In order to investigate the interaction of primary fuel combustion and boundary layer combustion, Fig. 19 shows the temperature contours at the $y = 0$ plane and part of the span of the scramjet engine obtained during simulations with different $\dot{m}_{Injector\_2}/\dot{m}_{Injector\_1}$ ratios. Compared with Case 2_combust_wo in Fig. 16(a), the temperature of Case 3 is the highest in the boundary layer near the upper wall of Injector_1, which indicates that when there is no boundary layer fuel, the area is fuel enriched combustion, and after some of the total fuel is separated keeping distribution ratio of $\dot{m}_{Injector\_2}/\dot{m}_{Injector\_1}$ as 1:4, the equivalent ratio here is very suitable for combustion, so the high temperature area is larger, and then, with the increase of fuel allocated to the boundary layer. The distribution ratio has changed from BSL (1:3) to Case 4 (1:2), which has become lean fuel again, so the high temperature area is less obvious compared to Case 3.

Fig. 20 depicts a succession of H_2 mass fraction contour plots at the following axial distance: $x = 0$, 0.3, 0.06, 0.09, 0.12, 0.18, 0.24 and 0.30 m within the combustor for different distribution ratios. The red areas on the contour plots represent H_2 mass fractions equal to or greater than 0.5. It can be seen that different distribution ratios have more significant effect on far field flow characteristics ($x > 0.09$ m) than near-field characteristics ($x < 0.09$ m), which could be derived in the more pronounced differences of the H_2 mass fraction contours at $x = 0.12$, 0.18 and 0.24 m. In Case 3, few boundary layer fuel exists, while the other two cases retain the consumption of the boundary layer fuel in the vicinity of outlet. Another remarkable distinction can be clearly seen is that the more injection of boundary layer fuel, the less volume of high temperature zone near the upper part of the expansion section along z direction. It is also worth noting that the above phenomenon merely occurs downstream.

The combustion efficiency along the flow path with different $\dot{m}_{Injector\_2}/\dot{m}_{Injector\_1}$ ratios is shown in Fig. 21 on the basis of considering its drag reduction efficiency. Basically, as the amount of fuel allocated to the Injector_1 is more than two times to that allocated to Injector_2, the combustion in the main flow is dominated by the primary fuel. So at the exit, the combustion efficiency values for all the three cases are almost the same and the maximum combustion efficiency can reach as high as 96% for Case 4. Interestingly, though in terms of skin-friction reduction, setting the

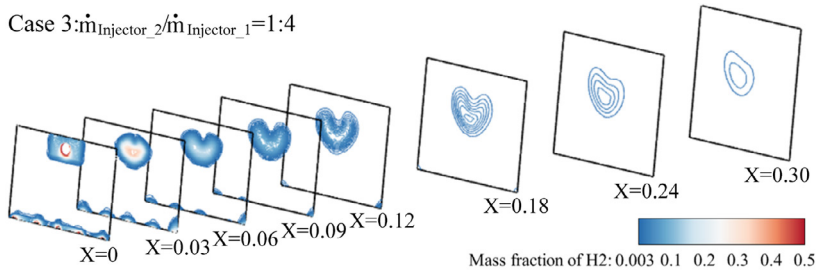

(a) Case 3

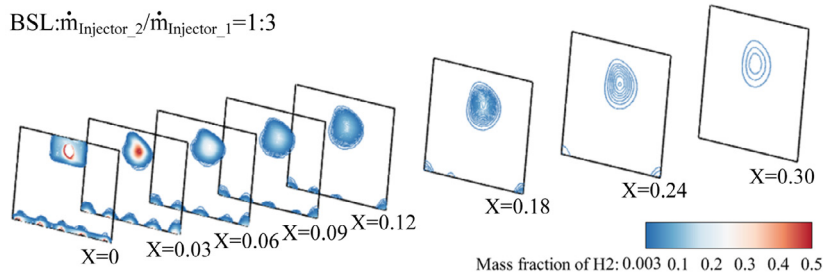

(b) BSL

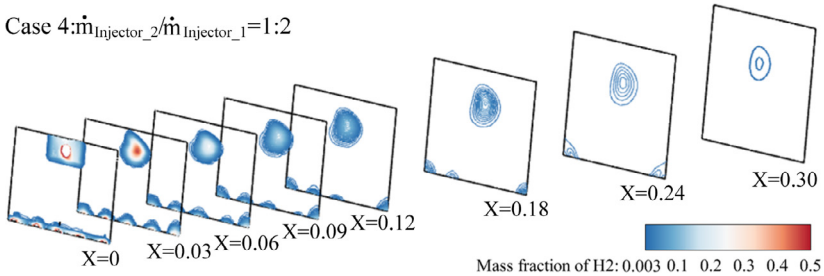

(c) Case 4

Fig. 20. Mass fraction of H_2 for different distribution ratio.

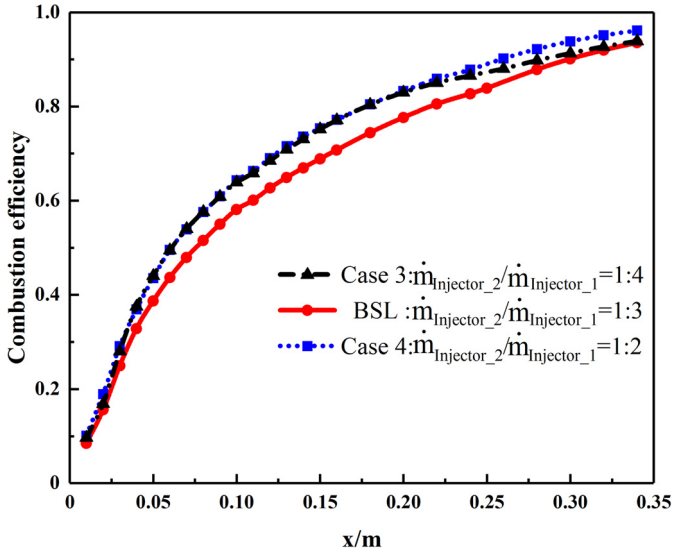

Fig. 21. Combustion efficiency along the flow path for different $\dot{m}_{Injector\_2}/\dot{m}_{Injector\_1}$.

value of $\dot{m}_{Injector\_2}/\dot{m}_{Injector\_1}$ ratio to 1:3 for BSL case is optimal. However, the combustion efficiency for BSL is consistently lower than that of other $\dot{m}_{Injector\_2}/\dot{m}_{Injector\_1}$ ratios such as Cases 3 and 4 along the flow path, and the maximum difference can reach to as high as 5% near $x = 0.175$ m. If the nozzle is not long enough, the overall combustion efficiency will be lower for the BSL case. Therefore, the addition of boundary layer combustion in scramjet combustor will be coupled with the combustion of the primary fuel. So trade-off study should be carried out to balance both the drag reduction performance and overall combustion performance in the combustor.

3.3. *Influence of different wall jet locations*

In this section, three locations along the flow path are chosen for investigating the effect of different wall jet device installing locations on the skin-friction reduction and combustion performance in combustor. From the study on different $\dot{m}_{Injector\_2}/\dot{m}_{Injector\_1}$ ratios above, it can be concluded that when the ratio is set as 1:3 for BSL case, the extent of drag reduction is maximum. Consequently, the $\dot{m}_{Injector\_2}/\dot{m}_{Injector\_1}$ ratio is kept constant at 1:3 when alternating the wall jet installation locations. Table 5 shows the different wall jet locations for BSL case, Cases 5 and 6. In Case 5, the wall jet fuel is injected at $x_0 = -0.05$ m, which is 0.05 m upstream of BSL injection point. Similarly, Case 6 represents that the wall jet device is installed at $x_0 = -0.1$ m, which is 0.1 m upstream of BSL case injection point.

Table 5
Inflow conditions and injection locations for BSL, Cases 5 and 6.

Parameter	Location	T_0 (K)	P_0 (kPa)	φ
BSL				
Injector_1	$X = 0$	297	709.94	0.260
Injector_2	$X = 0$	297	302	
Case 5				
Injector_1	$X = 0$	298.96	709.54	0.260
Injector_2	$X = -0.05$	298	301	
Case 6				
Injector_1	$X = 0$	297	709.46	0.260
Injector_2	$X = 0$–0.1	297	300	

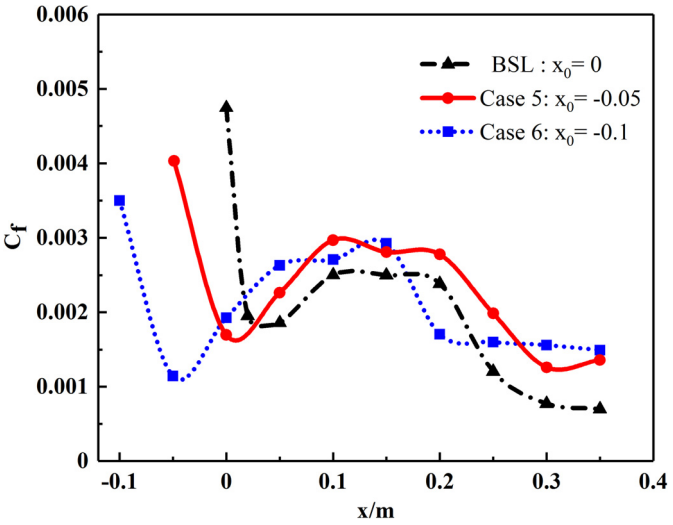

Fig. 22. Comparisons of C_f for different installation location of Injector_2.

Fig. 22 represents the skin-friction coefficient distribution on the lower wall for different injection locations. The variation of skin-friction coefficient can still be divided into a three-section developing process for different boundary layer fuel injection locations. There is no doubt that the closer the Injector_2 is installed to upstream, the earlier the friction coefficient decreases. For both Case 5 and Case 6, since their Injector_2 is installed upstream of the primary fuel injector ($x = 0$ m), the initial film-cooling effect is not disturbed by the primary fuel combustion. Compared to the BSL case in which the wall jet fuel mixing and combustion are coupled with the primary fuel combustion when the wall jet fuel is solely injected, the friction coefficient substantially increases for both Case 5 and Case 6 in the Reg. 2. As a result, the skin-friction coefficient is lower than that of both Case 5 and Case 6 at the downstream where boundary layer combustion plays a major role in drag reduction. Therefore, the installing position of wall jet device needs to be comprehensively measured by whether only film cooling or boundary layer combustion is deployed as the dominating role to reduce wall skin friction resistance.

To further investigate the interaction of flow near the lower wall and reveal the mechanism of the change trend of skin friction resistance, Fig. 23 shows the wall shear stress distribution on the lower wall for the three different wall jet injection locations separately. It is not difficult to find that there is a sudden drop in the wall shear stress near $x = 0.2$ m for Case 6 from Fig. 23(c). Meanwhile, the velocity gradient contour for this case along the flow path is also shown in Fig. 23(d). As the fluid temperature next to the lower wall increases, the density in this region consequently decreases, which result in a local dilatation of the fluid and increasing of boundary layer thickness. A thicker boundary layer leads to a smaller velocity gradient near the lower wall. In addition, from the above analysis, the relationship between wall shear stress and the velocity gradient can be recognized. It can be seen that the wall shear stress is reduced, which ultimately reduces the skin friction coefficient.

Moreover, an interesting phenomenon can be seen from the above two figures, the wall shear stress changes regularly and unevenly in the span direction (y direction). After the hydrogen is injected, due to the uneven mixing of hydrogen and air in the vicinity of the injector, the closer the injector is, the stronger the difference of the shear stress on the upper wall along the spanwise direction is. With the flow mixing, the difference of the shear stress in spanwise behind the flow field due to hydrogen injection gradually becomes smaller. Also due to the influence of front and rear walls, the wall shear stress of the test surface is generally higher in the middle than in the two sides. The wall shear stress of all injectors appear sharp convex ridges, which is followed by narrow valleys, while the middle exists smaller convex ridge. Moreover, the wall shear stress on the front and rear walls are very low, almost zero, which due to the no slip wall, those phenomena can be seen in local magnification in Fig. 23(c). The physical flow features observed in Case 6 could be also seen for the other case studies involving boundary layer combustion by wall jet injection.

Fig. 24 shows the comparison of combustion efficiency for different wall jet distance. From the plot, the combustion efficiency increases and then a sudden drop is observed. The initial increase represented by Reg. 1 indicates the combustion efficiency at the boundary layer combustion only. After the drop, the increase in combustion efficiency represented by Reg. 2 indicates the interactive effect of the primary and wall jet fuel. Advance of the installation location of wall jet device makes the boundary layer combustion more fully developed in isolator, which also leads to the phenomenon that the combustion efficiency in Case 6 is higher than the other two cases in the Reg. 1. Once combustion has commenced, however, it was noted that the combustion efficiency kept rising and tends to be consistent as the flow progressed in the x-direction under the coupling of primary and wall jet fuel.

Fig. 25 shows the contour of Mass fraction of OH along the flow path, compared with BSL and Case 5, the boundary layer fuel has been fully developed, resulting in the minimum shear stress in the lower wall shown in Fig. 23(c). Since the equivalence ratio is controlled at 0.260 in all three cases, when the wall jet device is advanced to $x_0 = -0.05$ m, especially close to the exit, the boundary layer combustion flame appears to gradually disappear due to the entrainment and combustion with the air outside the boundary layer. Moreover, the interference effect of primary fuel combustion on boundary layer combustion is stronger when the wall jet device continues to be moved forward to $x_0 = -0.1$ m. However, combined with the above analysis, these changes do not seem to have a great impact on combustion efficiency, which shows that the change of installation position of wall jet device can neither improve the combustion efficiency nor reduce the friction resistance.

4. Conclusions

A tangential slot injector is designed and added in a model scramjet engine to study the influence of boundary layer combustion for drag reduction. The useful conclusions can be drawn as follows:

1) Adding boundary layer combustion is an effective way for reducing skin friction in scramjet combustor. Meanwhile, the combustion efficiency could be increased as well. Through

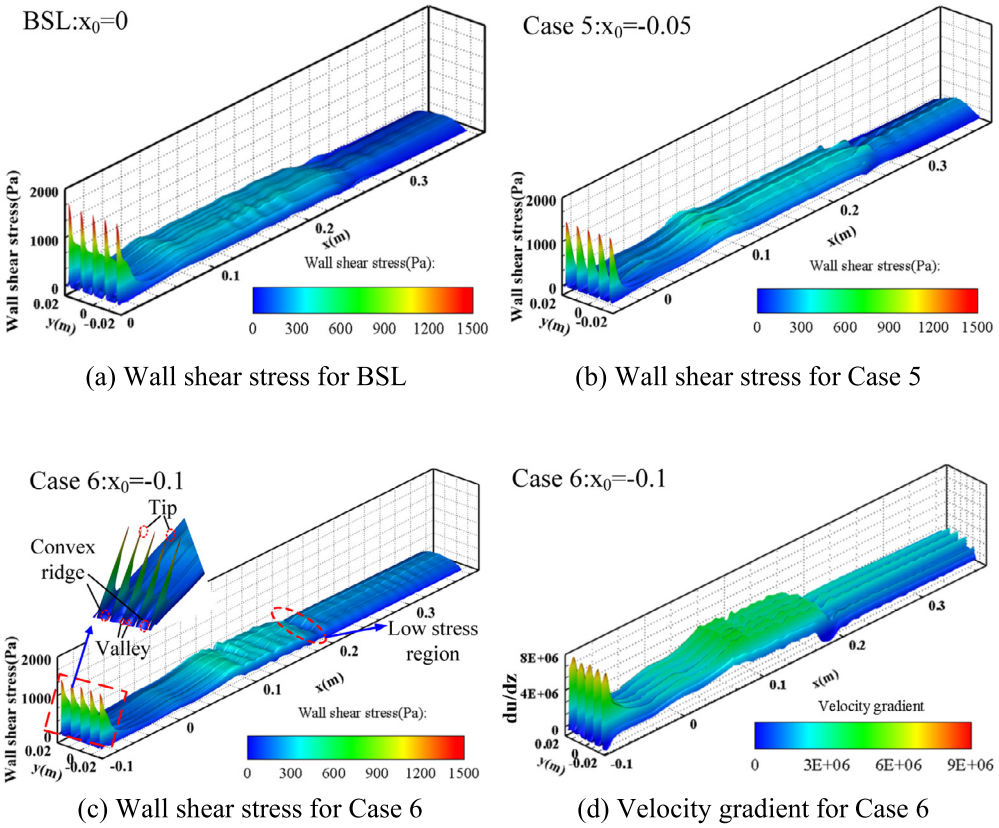

(a) Wall shear stress for BSL (b) Wall shear stress for Case 5

(c) Wall shear stress for Case 6 (d) Velocity gradient for Case 6

Fig. 23. Contour of wall shear stress and velocity gradient on the lower wall.

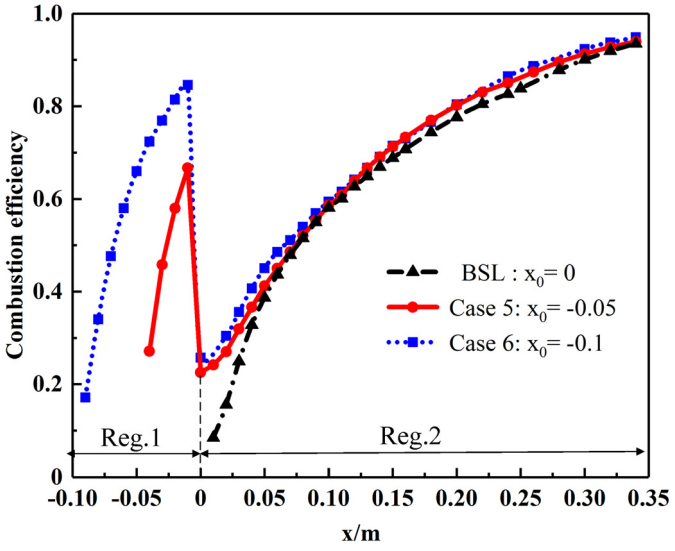

Fig. 24. Combustion efficiency along the flow path for different injection location.

boundary layer combustion, the wall friction resistance of scramjet engine could be reduced as large as 32% and combustion efficiency can be increased by 20%.

2) When the total amount of the fuel is kept constant, the distribution ratio of primary fuel which is used to produce thrust to the wall jet fuel has a little effect on the overall skin-friction reduction. Increasing the amount of wall jet fuel is beneficial to improve the drag reduction. However, due to the complex coupling between the combustion of the primary fuel and the wall jet fuel in these regions, the drag reduction does not increase monotonically with the injection of the wall jet fuel in the boundary layer.
3) The change of the installation position of the wall jet device has a great influence on the flow field especially in the area near the boundary layer. The upstream installation will make the interaction between the main combustion and the boundary layer combustion be stronger. However, this can not reduce the drag reduction rate and the combustion efficiency is not changed significantly. Hydrogen fuel injected into the cavity directly could improve the ignition performance greatly at the experimental status.

Declaration of competing interest

The authors declare that they have no known competing financial interests or personal relationships that could have appeared to influence the work reported in this paper.

Acknowledgements

This work was supported by the National Natural Science Foundation of China (Grant Number 51706170), China Postdoctoral Science Foundation (Grant Numbers 2019TQ0246, 2019M663734), Shaanxi Provincial Postdoctoral Science Foundation (Grant Number 2018BSHEDZZ03), the Foundation of State Key Laboratory of Coal Combustion (Grant Number FSKLCCA2004), Foundation of State Key Laboratory of High Temperature Gas Dynamics, and Fundamental Research Funds for the Central Universities (Grant Number xzy012019053).

References

[1] K. Ma, Z. Zhang, Y. Liu, Z. Jiang, Aerodynamic principles of shock-induced combustion ramjet engines, Aerosp. Sci. Technol. 103 (2020) 105901, https://doi.org/10.1016/j.ast.2020.105901.

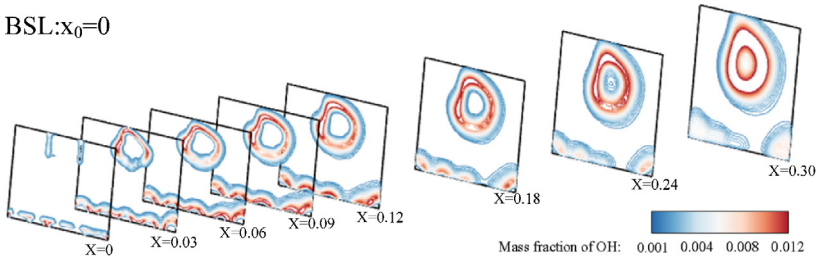

(a) BSL

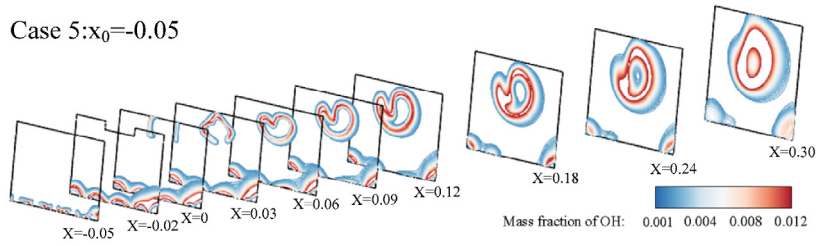

(b) Case 5

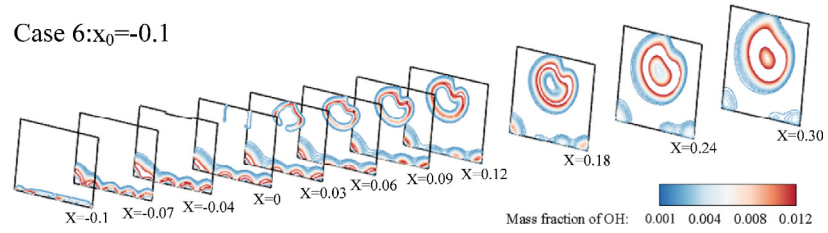

(c) Case 6

Fig. 25. Mass fraction of OH for different wall jet location.

[2] Z.G. Wang, M.B. Sun, H.B. Wang, et al., Mixing-related low frequency oscillation of combustion in an ethylene-fueled supersonic combustor, Proc. Combust. Inst. 35 (2015) 2137–2144, https://doi.org/10.1016/j.proci.2014.09.005.

[3] H. Wang, Z. Wang, M. Sun, et al., Combustion modes of hydrogen jet combustion in a cavity-based supersonic combustor, Int. J. Hydrog. Energy 38 (2013) 12078–12089, https://doi.org/10.1016/j.ijhydene.2013.06.132.

[4] W. Huang, L. Yan, Numerical investigation on the ram–scram transition mechanism in a strut-based dual-mode scramjet combustor, Int. J. Hydrog. Energy 41 (2016) 4799–4807, https://doi.org/10.1016/j.ijhydene.2016.01.062.

[5] C.P. Goyne, R.J. Stalker, A. Paul, C.P. Brescianini, Hypervelocity skin-friction reduction by boundary-layer combustion of hydrogen, J. Spacecr. Rockets 37 (6) (2000) 740–746, https://doi.org/10.2514/2.3645.

[6] J. Kostas, J.M. Foucaut, M. Stanislas, The effects of pulse frequency and duty cycle on the skin friction downstream of pulsed jet vortex generators in an adverse pressure gradient turbulent boundary layer, Aerosp. Sci. Technol. 13 (1) (2009) 36–48, https://doi.org/10.1016/j.ast.2008.03.002.

[7] R. Xue, X. Zheng, L. Yue, S. Zhang, C. Weng, Study of shock train/flame interaction and skin-friction reduction by hydrogen combustion in compressible boundary layer, Int. J. Hydrog. Energy 45 (31) (2020) 15683–15696, https://doi.org/10.1016/j.ijhydene.2020.04.027.

[8] E.R. Gowree, C. Jagadeesh, C.J. Atkin, Skin friction drag reduction over staggered three dimensional cavities, Aerosp. Sci. Technol. 84 (2019) 520–529, https://doi.org/10.1016/j.ast.2018.11.001.

[9] Y. Shkvar, S.A.E. Kryzhanovsky, Mathematical modeling of turbulent boundary layers, modified by wall-localized drag reduction techniques, Aerosp. Sci. Technol. 93 (2019) 105359, https://doi.org/10.1016/j.ast.2019.105359.

[10] S.J. Lee, Y.-G. Jang, Control of flow around a NACA 0012 airfoil with a micro-riblet film, J. Fluids Struct. 20 (5) (2005) 659–672, https://doi.org/10.1016/j.jfluidstructs.2005.03.003.

[11] H. Lu, Y. Yang, S. Guo, W. Pang, F. Yang, J. Zhong, Control of corner separation via dimpled surface for a highly loaded compressor cascade under different inlet Mach number, Aerosp. Sci. Technol. 85 (2019) 48–60, https://doi.org/10.1016/j.ast.2018.11.054.

[12] K. Satheesh, G. Jagadeesh, Effect of electric arc discharge on hypersonic blunt body drag, Shock Waves (2009) 577–582, https://doi.org/10.1007/978-3-540-85168-4_92.

[13] R.J. Stalker, Control of hypersonic turbulent skin friction by boundary-layer combustion of hydrogen, J. Spacecr. Rockets 42 (4) (2005) 577–587, https://doi.org/10.2514/1.8699.

[14] E.R.V. Driest, Turbulent boundary layer in compressible fluids, J. Aeronaut. Sci. 18 (3) (1951) 145–160, https://doi.org/10.2514/8.1895.

[15] J.E. Barth, V. Wheatley, M.K. Smart, Hypersonic turbulent boundary-layer fuel injection and combustion: skin-friction reduction mechanisms, AIAA J. 51 (9) (2013) 2147–2157, https://doi.org/10.2514/1.J052041.

[16] H. Wang, Z. Wang, M. Sun, et al., Flame characteristics in supersonic combustor with hydrogen injection upstream of cavity flameholder, Proc. Combust. Inst. 34 (2013) 2073–2082, https://doi.org/10.1016/j.proci.2012.06.049.

[17] M. Sun, H. Geng, J. Liang, et al., Flame characteristics in supersonic combustor with hydrogen injection upstream of cavity flameholder, J. Propuls. Power 24 (2008) 688–696, https://doi.org/10.2514/1.34970.

[18] S. Rowan, Viscous drag reduction in a scramjet combustor, Ph.D. thesis, Department of Mechanical Engineering, the University of Queensland, St Lucia, Queensland, Australia, 2003.

[19] M.V. Suraweera, D.J. Mee, R.J. Stalker, Skin friction reduction in hypersonic turbulent flows by boundary-layer combustion, in: 43rd AIAA Aerospace Sciences Meeting and Exhibit, Reno, Nevada, 10-13 January, 2005, AIAA Paper 2005-0613.

[20] R.J. Clark, S.O. Bade Shrestha, Boundary layer combustion for skin friction drag reduction in scramjet combustors, in: 50th AIAA/ASME/SAE/ASEE Joint Propulsion Conference, Cleveland, OH, 28-30 July, 2014, AIAA Paper 2014-3667.

[21] E.P. Volchkov, V.V. Lukashov, Experimental study of characteristics of a laminar boundary layer with hydrogen combustion, Combust. Explos. Shock Waves 48 (4) (2012) 375–381, https://doi.org/10.1134/S0010508212040016.

[22] P. Zhang, J. Xu, Y. Yu, W. Cui, Effect of adverse pressure gradient on supersonic compressible boundary layer combustion, Aerosp. Sci. Technol. 88 (2019) 380–394, https://doi.org/10.1016/j.ast.2019.03.013.

[23] R. Xue, X. Zheng, L. Yue, S. Zhang, C. Weng, Numerical study on supersonic boundary-layer transition and wall skin friction reduction induced by fuel wall

jet combustion, Acta Astronaut. 174 (2020) 11–23, https://doi.org/10.1016/j.actaastro.2020.04.031.
[24] M. Trenker, D.J. Mee, R.J. Stalker, Reducing skin friction by boundary layer combustion on a generic scramjet mode, in: Z. Jiang (Ed.), Shock Waves, Springer, Berlin, Heidelberg, 2005, pp. 903–908.
[25] S. Rowan, A. Paull, Viscous drag reduction in a scramjet combustor with film cooling, in: 10th AIAA/NAL/NASDA/ISAS International Space Planes and Hypersonic Systems and Technologies Conference, Kyoto, Japan, 24-27 April, 2001, AIAA Paper 2001-1818.
[26] R.M. Kirchhartz, D.J. Mee, R.J. Stalker, Supersonic skin-friction drag with tangential wall slot fuel injection and combustion, AIAA J. 50 (2) (2012) 313–324, https://doi.org/10.2514/1.J051073.
[27] W.Y.K. Chan, D.J. Mee, M.K. Smart, J.C. Turner, R.J. Stalker, Boundary layer combustion for viscous drag reduction in practical scramjet configurations, in: 27th International Congress of the Aeronautical Sciences, Nice, France, January, 2010, pp. 1–10, https://espace.library.uq.edu.au/view/UQ:228181.
[28] W.Y.K. Chan, D.J. Mee, M.K. Smart, J.C. Turner, Drag reduction by boundary-layer combustion: effects of flow disturbances from rectangular-to-elliptical-shape-transition inlets, J. Propuls. Power 31 (5) (2015) 1256–1267, https://doi.org/10.2514/1.B35335.
[29] W.Y.K. Chan, D.J. Mee, M.K. Smart, J.C. Turner, Drag reduction by boundary-layer combustion: influence from disturbances typical of cross-stream fuel-injection, J. Propuls. Power 31 (5) (2015) 1486–1491, https://doi.org/10.2514/1.B35665.
[30] S. Wang, G.-q. He, D.-k. Yan, Z.-w. Huang, F. Qin, Analysis and reduction of skin-friction in a rocket-based combined-cycle engine flow path operating from Mach 1.5 to 6.0, Acta Astronaut. 151 (2018) 357–367, https://doi.org/10.1016/j.actaastro.2018.06.028.
[31] N.M. Marinov, C.K. Westbrook, W.J. Pitz, Detailed and global chemical kinetics model for hydrogen, in: 8th International Symposium on Transport Processes, San Francisco, CA (United States), Oct. 1995, https://www.osti.gov/servlets/purl/90098.
[32] Z. Huang, G. He, F. Qin, X. Wei, Large eddy simulation of strut enhanced mixing for supersonic combustion, J. Solid Rocket Technol. 38 (5) (2015) 664–670, https://doi.org/10.7673/j.issn.1006-2793.2015.05.012.
[33] A.B. Vishal, A.V. Manan, A.E. William, J.G. Nicholas, Numerical simulation of vitiation effects on hydrogen-fueled dual-mode scramjet, in: 48th AIAA Aerospace Sciences Meeting Including the New Horizons Forum and Aerospace Exposition, Orlando, Florida, 04-07 January, 2010, AIAA 2010-1127.